ARL-CR-0810 ● DEC 2016

US Army Research Laboratory

Aerodynamic Optimization of a Supersonic Bending Body Projectile by a Vector-Evaluated Genetic Algorithm

prepared by Justin L Paul
Academy of Applied Science
24 Warren Street
Concord, NH 03301

under contract W911SR-15-2-001

NOTICES

Disclaimers

The findings in this report are not to be construed as an official Department of the Army position unless so designated by other authorized documents.

Citation of manufacturer's or trade names does not constitute an official endorsement or approval of the use thereof.

Destroy this report when it is no longer needed. Do not return it to the originator.

ARL-CR-0810 ● DEC 2016

US Army Research Laboratory

Aerodynamic Optimization of a Supersonic Bending Body Projectile by a Vector-Evaluated Genetic Algorithm

prepared by Justin L Paul
Academy of Applied Science
24 Warren Street
Concord, NH 03301

under contract W911SR-15-2-001

REPORT DOCUMENTATION PAGE

Form Approved
OMB No. 0704-0188

1. REPORT DATE *(DD-MM-YYYY)*	2. REPORT TYPE	3. DATES COVERED (From - To)
December 2016	Contractor Report	1 June–31 August 2016

4. TITLE AND SUBTITLE
Aerodynamic Optimization of a Supersonic Bending Body Projectile by a Vector-Evaluated Genetic Algorithm

5a. CONTRACT NUMBER
W199SR-15-2-001

5b. GRANT NUMBER

5c. PROGRAM ELEMENT NUMBER

6. AUTHOR(S)
Justin L Paul

5d. PROJECT NUMBER
AH80

5e. TASK NUMBER

5f. WORK UNIT NUMBER

7. PERFORMING ORGANIZATION NAME(S) AND ADDRESS(ES)
Academy of Applied Science
24 Warren Street
Concord, NH 03301

8. PERFORMING ORGANIZATION REPORT NUMBER

9. SPONSORING/MONITORING AGENCY NAME(S) AND ADDRESS(ES)
US Army Research Laboratory
ATTN: RDRL-WML-E
Aberdeen Proving Ground, MD 21005-5066

10. SPONSOR/MONITOR'S ACRONYM(S)

11. SPONSOR/MONITOR'S REPORT NUMBER(S)
ARL-CR-0810

12. DISTRIBUTION/AVAILABILITY STATEMENT
Approved for public release; distribution is unlimited.

13. SUPPLEMENTARY NOTES

14. ABSTRACT
Computational fluid dynamics (CFD) and evolutionary programming were used to start the process of finding the optimal geometries of a bending body variation of the US Air Force Finner—a 30-mm-diameter, 300-mm-long, fin-stabilized projectile—for a range of angles of attack at 3 supersonic Mach numbers. Three analysis tools were evaluated for simulating aerodynamic coefficients associated with the configurations to be optimized: CFD++ by Metacomp Technologies, SOLIDWORKS Flow Simulation, and Missile Datcom. The analysis tool chosen for this research was CFD++. The configurations were optimized for control authority and drag considerations at each angle of attack and Mach number using a genetic algorithm. The optimization search space is composed of 3 control parameters: the angular deflection of the nose cone, the angular deflection of the body, and the location of the body angular deflection. A vector-evaluated genetic algorithm was written to guide generations of configurations toward the optimal configuration for a given angle of attack and Mach number using the aerodynamic coefficients obtained from the CFD simulations completed on the previous generation of configurations.

15. SUBJECT TERMS
bending body, aerodynamic coefficients, genetic algorithm, optimization, maneuverability

16. SECURITY CLASSIFICATION OF:			17. LIMITATION OF ABSTRACT	18. NUMBER OF PAGES	19a. NAME OF RESPONSIBLE PERSON
a. REPORT	b. ABSTRACT	c. THIS PAGE			Sidra Silton
Unclassified	Unclassified	Unclassified	UU	38	19b. TELEPHONE NUMBER (Include area code) 410-306-0792

Contents

List of Figures

List of Tables

Acknowledgments

The author would like to thank the following individuals: Dr Sidra Silton of the Flight Sciences Branch (FSB) for her mentorship, consultation, and guidance; Mr Ilmars Celmins of the FSB for his assistance with SOLIDWORKS; and Mr Bryant Nelson of the Guidance Technologies Branch for initial concept development and evolutionary programming conceptualization. This investigation used significant computational resources from the US Department of Defense (DOD) High Performance Computing Modernization Program located at the US Navy DOD Supercomputing Resource Center at Stennis Space Center, Mississippi.

INTENTIONALLY LEFT BLANK.

1. Introduction

A bending body projectile is a maneuver technology concept being investigated for the small-diameter munitions research area. This research area is part of the US Army Research Laboratory's Science for Lethality and Protection Campaign. The Army is concerned with munitions capable of both precision and accuracy to minimize collateral damage and maximize lethal effects. Bending body technology may enable projectiles to achieve the required control authority necessary to achieve this goal.[1]

Current maneuvering munitions rely on moving control surfaces (e.g., canards or fins), reaction control jets, or thrust vectoring for their control authority. Canards are currently the most common method of control for gun-launched projectiles. Although canards have proven effective for some missions, bending body technology offers the potential for even greater control authority, which would improve performance and increase mission versatility. Bending body technology may be advantageous compared with moving control surfaces for multiple reasons: less drag when not maneuvering as there are no external control surfaces, no canard-induced aerodynamic issues,[1–4] structural integrity during launch, and volumetric constraints with associated launch platforms.

Past research on deflectable projectile structure has been primarily concerned with deflecting the nose cone at its base.[5–6] Landers et al.[5] investigated aerodynamic stability and pitch control effectiveness of a hypervelocity projectile with a deflectable nose as compared with canard controls for a projectile with a large length-to-diameter ratio. Shoesmith et al.[7] conducted a computational investigation of aerodynamic characteristics for a supersonic projectile with deflectable nose control. Both of these investigations found that a deflectable nose could provide control authority at supersonic velocities but were limited in both angle of attack (α) range and nose deflection angle range. Youn and Silton[1] investigated the effective control of a deflectable nose cone as well as a body deflection for a supersonic projectile. In addition to a second bend, a larger range of angles of attack was considered as well as significantly larger deflection angles. The additional bend demonstrated increasing control authority at the cost of increased drag. The current investigation expands on this concept by seeking to optimize the control parameters associated with the deflections.

The challenge with optimizing the bending body projectile problem is the highly dimensional, multimodal nature of the problem. Simple optimization techniques such as Golden section search or Newton–Raphson method are not compatible or are impractical to implement. Li et al.[8] demonstrated that evolutionary programming can be used for aerodynamically driven shape optimization. Many

other researchers and scientists have demonstrated similar investigations.[9–11] Evolutionary programming is a powerful optimization technique that is widely applicable to scientific research and engineering industry. As a subset of machine learning, evolutionary programming provides a robust approach to the difficult optimization task.

The evolutionary programming technique used in this investigation is a genetic algorithm. A genetic algorithm evolves multiple generations of a population of individuals where each individual is a "solution" to the problem or objective function. The objective function characterizes what is being optimized. Individuals that are found to solve the problem poorly are progressively removed from future generations, while those found to solve the problem well thrive in future generations. The algorithm iterates until a convergence condition is met.[8–12] Defining aspects of genetic algorithms include metaheuristic, stochastic, and conditionally global. Genetic algorithms are metaheuristic because they find practical solutions instead of exact or perfect solutions. They are stochastic because elements of the algorithm use pseudo-random number generation techniques. Finally, they are conditionally global depending on how the algorithm is constructed. If the algorithm is not properly constructed, there may not be enough diversity in the generations to search the entire design space of the problem. This issue results in optimized individuals finding local extrema instead of global extrema.

In the current investigation, an individual is a particular configuration of the projectile. Simulations of the configurations are completed to evaluate how well they solve the objective function. The objective function is an equation set that evaluates the performance of individuals. Successive generations are made to emphasize well-performing individuals through performance-based selection and recombination. Although well-performing individuals are given greater attention, it is not necessarily guaranteed that future generations will always produce better-performing individuals. The theory is that with enough iterations of the algorithm and a large, diverse sample population, performance across individuals will generally increase.

Using a genetic algorithm, the current investigation seeks to identify optimal bending body configurations for a supersonic projectile that maximize maneuverability while minimizing drag. These optimal configurations are found for each case (α and freestream Mach number, M_∞) considered in the test matrix. This matrix, to be described later, consists of 51 different cases.

2. Projectile Design

The projectile being studied is the Air Force Finner (AFF): a 30-mm diameter (*D*), fin-stabilized projectile. This projectile was chosen because it is a baseline supersonic geometry that has been studied extensively with copious computational and empirical data available for comparison.[13–18] The projectile has 4 clipped delta fins on the end of the projectile spaced equidistant about its axis. The fins are uncanted and parallel with the projectile's axis. The supersonic projectile has a length-to-diameter ratio of 10 and the nose cone length is 2.5 *D*. The fins are beveled on the leading and trailing edges with a root cord of $\frac{4}{3}$ *D* and a semispan of 0.5 *D*. The baseline straight body configuration is shown in Fig. 1.

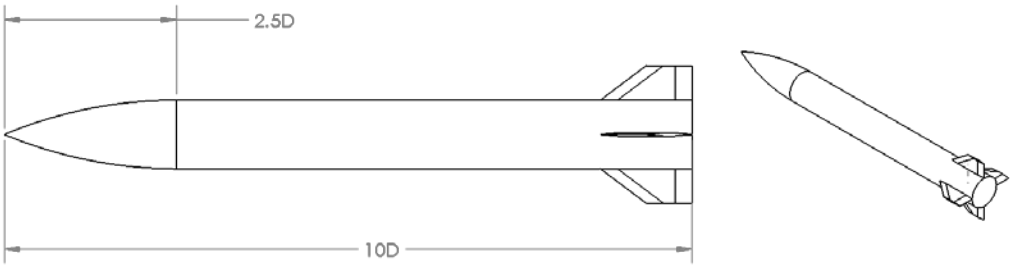

Fig. 1 Baseline straight body configuration

The projectile is designed to fly in the baseline straight body configuration and morph into in a bent body configuration when a maneuver is commanded. A generic bent body configuration is shown in Fig. 2 with control parameters Φ_1, Φ_2, and Q_1. The first bend (Φ_1) is located at the base of the nose cone, and the second bend (Φ_2) is located between the base of the nose cone and the projectile's center of gravity (CG). The location of the second bend (Q_1) is allowed to vary between 1.25 and 68.75 mm from the CG in 4.5-mm increments. The bend angles (Φ_1 and Φ_2) are permitted to vary from 0° to 7.5° in 0.5° increments.

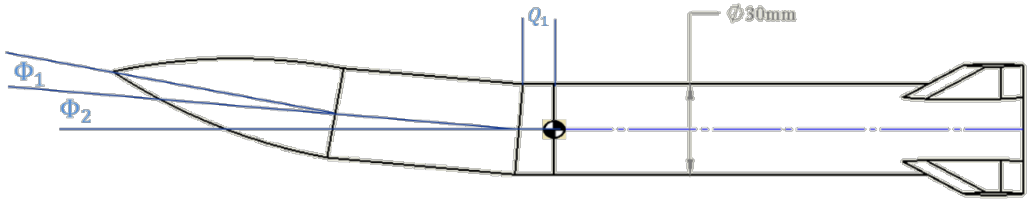

Fig. 2 Generic bent body configuration

Angle of attack of the projectile is defined as the angle between the freestream velocity vector and the trajectory vector of the projectile. The trajectory of the projectile in the straight and bent body configuration can be taken as the axial direction of the portion of the projectile behind the CG. The tail of the trajectory vector would be located aft of the projectile, and the head of the vector would be located at the CG. All of the cases for each α are completed at Mach 2, Mach 3, and Mach 4 for standard sea level temperature and pressure (298 K, 101,325 Pa).

3. Methodology

3.1 Simulation Methods Explored

Aerodynamic coefficients must be obtained for each configuration to evaluate the performance. Since a large number of configurations are being investigated, it is necessary to select the most accurate and efficient method to determine these coefficients. Three simulation methods were considered for this investigation: Missile Datcom,[19] SOLIDWORKS Flow Simulation,[20] and CFD^{++} by Metacomp Technologies.[21]

Missile Datcom is an aero-prediction code that uses a hybrid of empirical and analytical techniques to calculate aerodynamic coefficients. This solver has the advantage of expedited analysis compared with other solvers by several orders of magnitude. This advantage is made at a cost of limited modeling capability and accuracy. Limited accuracy was determined by comparing Missile Datcom results with CFD^{++} results for the baseline (straight body) projectile geometry analyzed by Youn and Silton.[1] Data were compared at 5 angles of attack between –12° and 12°. Axial force coefficient (C_X) was predicted within 12%, even at Mach 4, and normal force coefficient (C_N) predicted within 18% across the Mach number range (Fig. 3). However, pitching moment coefficient (C_m) was not well predicted at all, with errors in excess of 30% for most of the cases compared. The exception was for low angles of attack at Mach 2. This was of concern as C_m has a large effect on maneuverability. Analysis of the cause of the discrepancy in pitching moment coefficient was not conducted, as it was unclear at the time if it would be possible to model a bending body geometry within Missile Datcom.

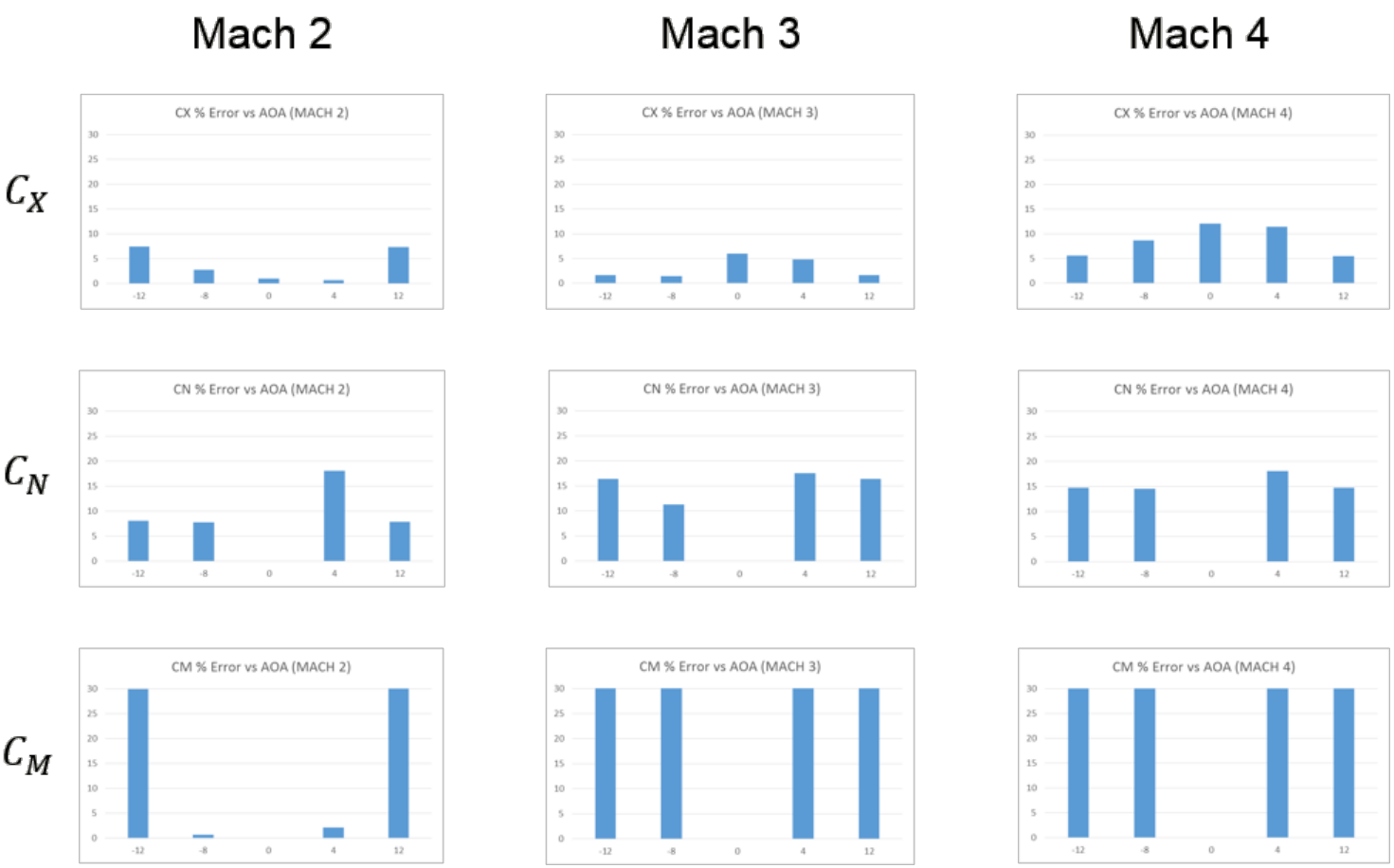

Fig. 3 Percent error difference between Missile Datcom and CFD^{++} results for projectile geometry in Youn and Silton[1]

SOLIDWORKS Flow Simulation is a computational fluid dynamics (CFD) solver embedded in a computer-aided design (CAD) software. Using CAD software, this solver has virtually unbounded modeling capability. This advantage also provides meshing that is expedited by the embedded nature of the solver. Simulation time and accuracy, however, scale with mesh refinement. In addition, limited licenses were available and simulations can only be run on a computer under the Windows operating system. These disadvantages together translate to an impractical time requirement for simulations. Results from SOLIDWORKS Flow Simulation were also compared with the CFD^{++} results from Youn and Silton[1] (Fig. 4). The comparison was made with the same methodology as the comparison made in Fig. 3. Interestingly, the data comparison also results in the pitching moment coefficient being the least accurate. It is important to mention that to achieve practical simulation time, the mesh used for the SOLIDWORKS simulations was a significantly smaller size at just 150,000 cells. It is likely that a larger mesh size (similar to meshes used for CFD^{++}) would increase accuracy.

The final simulation method explored was the commercial software CFD^{++} by Metacomp Technologies. This is a stand-alone CFD analysis tool that accepts mesh files from its partner commercial software MIME (Multipurpose Intelligent Meshing Environment) which accepts native CAD geometry.[22] MIME permits CFD^{++} to have virtually unbounded modeling capabilities similar to that of SOLIDWORKS Flow Simulation. As with SOLIDWORKS Flow Simulation, time requirements and accuracy scale with mesh refinement. Because CFD^{++} is available on the US Department of Defense (DOD) High Performance Computing Modernization Program (HPCMP), licensing and computational resources were not restrictive. Although validation studies were not completed on the AFF geometry for the mesh considered in the present paper, CFD^{++} has previously been used with sufficient accuracy for the AFF on a different mesh in the Mach regime investigated in this study.[17,18] The current mesh is similar to that of Youn and Silton.[1] The advantage of CFD^{++} over Missile Datcom, although significantly more consuming of resources, is the versatility of geometry as well as the ability to analyze the flow field as well as the aerodynamic coefficients, which were shown previously only to be predicted adequately at best for this geometry. Considering the advantages and disadvantages for each simulation method, CFD^{++} was selected as the suitable simulation method.

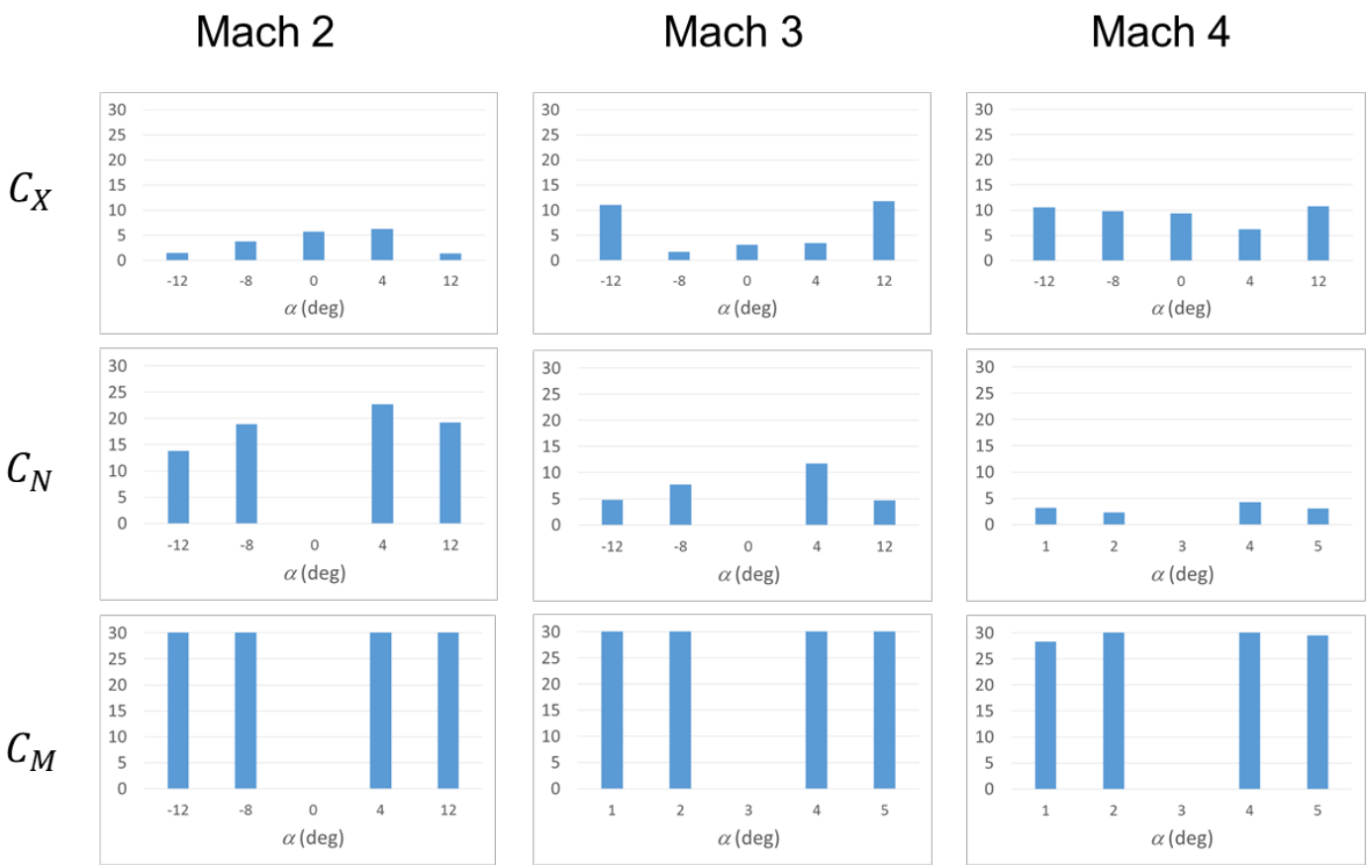

Fig. 4 Percent error difference between SOLIDWORKS Flow Simulation results and CFD^{++} results from Youn and Silton[1]

3.2 CFD Methodology

All computational meshes were created using MIME.[22] Longitudinal symmetry was taken advantage of to reduce the total mesh size by a factor of 2. A typical size for a configuration's global mesh was 9.1–12 million cells. The surface mesh on the body was created using Delaunay triangulation and the growth rate was restricted to 1.4. A close-up of the fin region can be seen in Fig 5. The cells close to the surface and within the boundary layer were prism cells while cells in the far field were tetrahedrals. Figure 6 shows a close-up of the boundary layer region. A boundary layer spacing of 1e-6 m with a growth rate of 1.2 was chosen such that the nondimensional wall distance was approximately 1. The growth rate of the tetrahedrals was also 1.4. Figure 7 shows a global mesh for individual 28 from generation 1. Density boxes were used around the body and in the wake to control mesh growth for adequate resolution of the shock and wake regions.

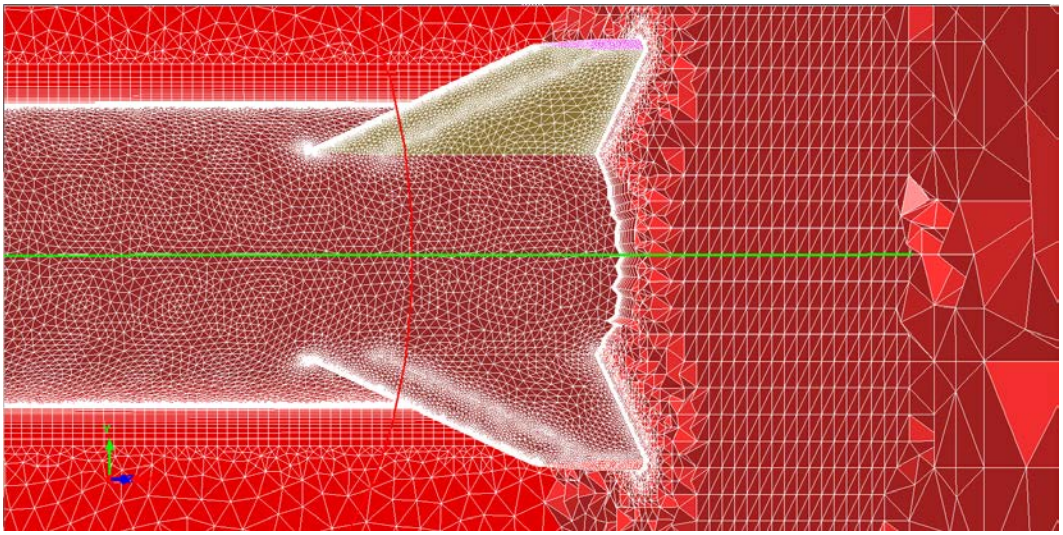

Fig. 5 A 3-D cut plane of fin region cells

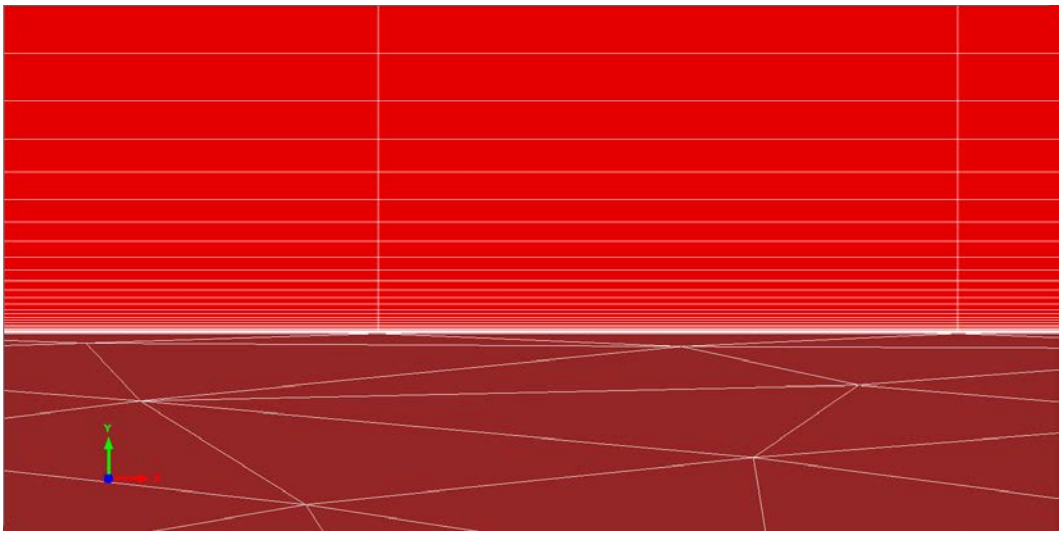

Fig. 6 Boundary layer size

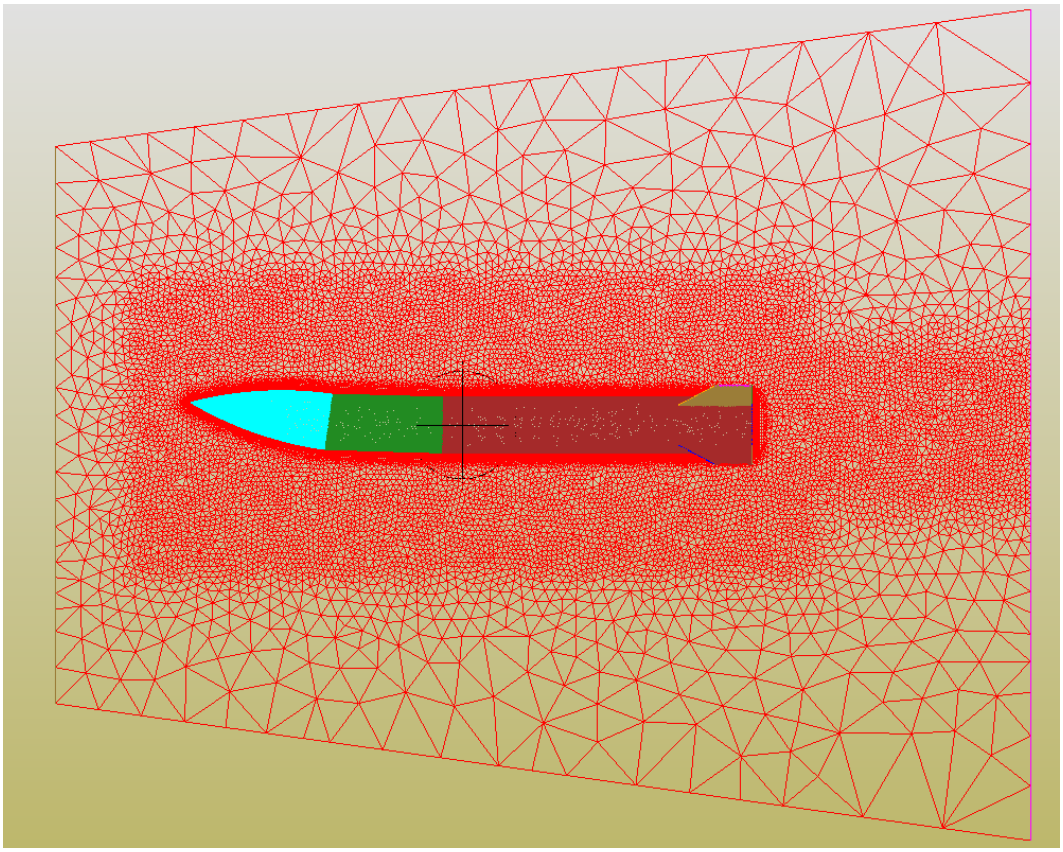

Fig. 7 Individual 28 from generation 1

All configurations were simulated using the Reynolds-averaged Navier–Stokes equation set with the realizable k-ε turbulence closure model. All simulations used air at standard temperature and pressure at sea level altitude for freestream fluid properties. The simulations were started at α = –8° as a steady-state case, and then swept up in 0.25° increments as transient, quasi-steady simulations until α = 8° using the methodology described by Sahu and Heavey[23] and Youn and Silton.[1] A 0.25° increment is necessary to ensure convergence of the quasi-steady simulations; only 1° increments are analyzed. The baseline straight body configuration was simulated as one of the individuals. Each mesh was partitioned into 96 different parts and simulated on Conrad, a Cray XC40 supercomputer located at the Navy DOD Supercomputing Resource Center at Stennis Space Center, Mississippi. Simulations for the complete range of angles of attack typically required 6–10 h for completion. The data collected from these simulations and used for optimization were pitching moment coefficient, axial force coefficient, and normal force coefficient. These coefficients are shown in Eqs. 1–3.

$$C_m = \frac{M}{\frac{1}{2}\gamma p_\infty {M_\infty}^2 SD} \quad , \tag{1}$$

$$C_X = \frac{F_X}{\frac{1}{2}\gamma p_\infty {\mathrm{M}_\infty}^2 S} \quad , \tag{2}$$

$$C_N = \frac{F_N}{\frac{1}{2}\gamma p_\infty {\mathrm{M}_\infty}^2 S} \quad , \tag{3}$$

where M is the pitching moment, F_X is the axial force, F_N is the normal force, γ is the gas constant for air (1.4), p_∞ is freestream pressure, M_∞ is freestream Mach number, and S is the area of the projectile.

3.3 The Vector-Evaluated Genetic Algorithm

The genetic algorithm is the tool used to optimize the shape of the different configurations. Each configuration is considered an individual in a population within a generation. These individuals are represented as a set of the 3 control parameters $\Phi_1, \Phi_2,$ and Q_1. As a normalized set, each control parameter has a design space within a set of 16 bins. As integers, each control parameter is permitted to vary between 1 and 16. Within the algorithm, these individuals are converted from a set of 3 control parameters to a string of binary bits. Each control parameter is represented as 4 bits; therefore, an individual is represented at 12 bits. Each bit is referred to as a nucleotide. The complete string of nucleotides of an individual is called the genotype. The physical manifestation of the genotype (control parameters) is the phenotype (projectile shape). A sample genotype is shown in Fig. 8. All of the algorithm parameters and properties are listed in Table 1.

Each of the parameters will be discussed in greater detail in Sections 3.3.1 through 3.3.4.

Fig. 8 A sample genotype

Table 1 Algorithm parameters and properties

Initial population size	31
Intermediate population size	6
Priority coefficient vector	<(1/2) , (1/3) , (1/6)>
Natural selection cutoff	50%
Crossover rate	70%
Mutation rate	5%
Confidence interval	90%

3.3.1 The Objective Function

The genetic algorithm in this investigation is vector evaluated because the objective function is a weighted linear combination of goals creating a single metric of performance for an individual.[12,24] The priority coefficient vector is how the goals (in this case the aerodynamic coefficients) are to be weighted. The aerodynamic coefficients considered as part of the priority coefficient vector are C_m at 1/2, C_X at 1/3, and C_N at 1/6. These priority coefficients were chosen based on the importance of maximizing maneuverability and minimizing drag.

To understand how this represents the physical performance of an individual, the objective function must be broken into smaller parts starting with a given set of aerodynamic coefficients from a generation of simulations. The objective function encompasses every calculation and measurement that is used to determine the geometry and aerodynamic coefficients, as well as those used to perform the optimization. The portions of the objective function that are based on physics (e.g., aerodynamic coefficients as determined by the CFD simulations) cannot be changed. Thus, only the portion of the objective function that has been created for this investigation (the genetic algorithm) will be discussed.

The first step in the genetic algorithm is to determine the set size for each of the aerodynamic coefficients being considered (Eq. 4). The set size is determined by

the maximum (max) and minimum (min) values of the aerodynamic coefficient set. The data niche is the difference between coefficient values of the individuals required to make them unique. For example, if the maximum C_m is 2.02 and the minimum C_m is –1.09 for a given generation at a particular M_∞ and α and the niche size is chosen as 0.01 (i.e., the values of C_m must differ by more the 0.01 to be considered unique), the set size is 311.7. The value score (Eq. 5) of each individual is determined by taking the value of the corresponding aerodynamic coefficient (value) and comparing it with the size and maximum value of the coefficient set. Therefore, if a given individual has a C_m value of 0.49, that individual would have a value score of 75.4. Value score equation structure normalizes fitness metrics and scales with their "relative impact" on aerodynamic performance. The value score is maximized for C_m and C_N.

$$set \equiv \{min: niche: max\}, \quad size = \frac{max - min}{niche} \tag{4}$$

$$value\ score = \frac{value}{max} * size \tag{5}$$

The value score equation (Eq. 5) permits the algorithm to determine the tradeoff between the aerodynamic coefficients impact on the score of an individual. If a particular coefficient set has a smaller size (Eq. 4) compared with another coefficient set, it has less of an impact on the shape of the configurations and is reflected in the respective value scores of those coefficients. Each value score is then scaled by its priority coefficient to create its component score. The component scores are summed to create the final fitness score. The linear combination of component scores is what makes this algorithm vector evaluated.[12,24] These concepts are shown in Eqs. 6 and 7. To normalize the set of fitness scores, each score is divided by the maximum score within the set. The result is a set of fitness-proportionate values for each individual (Eq. 8).

$$component\ score = priority\ coefficient * value\ score \tag{6}$$

$$final\ fitness\ score = \sum_{j=1}^{N} (component\ score)_j \tag{7}$$

$$fitness\ proportionate\ probability = \frac{(final\ fitness\ score)_i}{maximum\ final\ fitness\ score} = \frac{w_i}{w_{max}} \tag{8}$$

A slight modification of the value score equation is required to achieve minimization, as is necessary for C_X. This modification is shown in Eq. 9. Using this modification, the value score increases for decreasing aerodynamic coefficient value. This is how minimization and maximization can be considered simultaneously in vector evaluation.

$$value\ score = \frac{min}{value} * size \tag{9}$$

3.3.2 Selection

Selection comprises 2 phases: natural and parental. Natural selection is simply finding the median fitness score in the population and then removing all of the corresponding individuals at or below this threshold (the natural selection cutoff). The resulting population is considered the fit population. Parental pairs are then selected from the fit population. Parental selection is guided by fitness proportionate probability with stochastic acceptance[25–27] also known as roulette wheel selection. An individual is first selected with uniform probability. The probability an individual is selected as a parent is based on its fitness-proportionate value. This concept is shown in Fig. 9, where x in this figure is the chosen fitness-proportionate value.

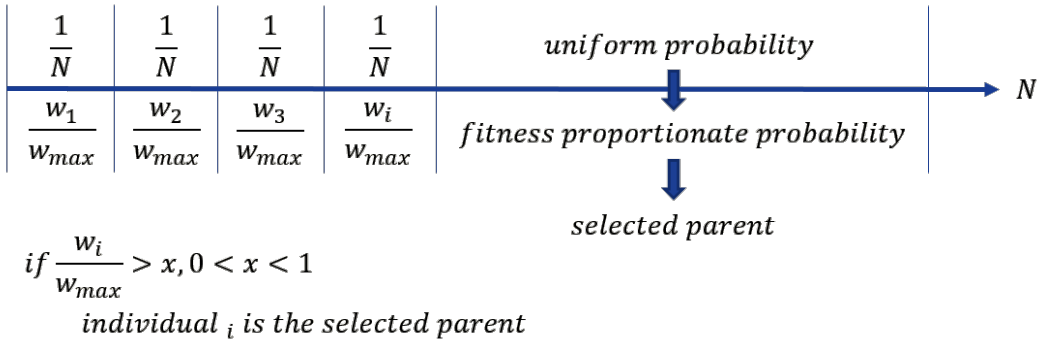

Fig. 9 Parental selection

3.3.3 Recombination

Recombination comprises 2 phases: crossover and mutation. Crossover recombination is hybrid genotype resulting from the hybridization of 2 parent individuals. The nucleotides that form each individual are swapped at a random location to create the new individual (Fig. 10). Each offspring has some probability of not using crossover (crossover rate), in which case, the first parent in the parental pair is selected as the offspring (i.e., cloned). Once the offspring is generated, it is then subject to mutation at the mutation rate. In mutation recombination, each nucleotide in an offspring's genotype is subject to change. This recombination process is demonstrated in Figs. 10 and 11.

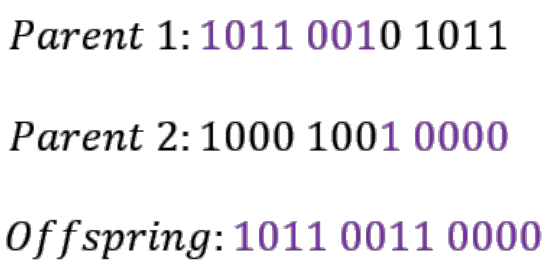

Fig. 10 Crossover

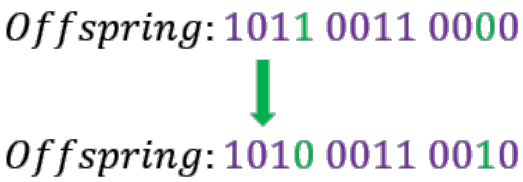

Fig. 11 Mutation

Mutation occurs with drastically lower probability compared with crossover (Table 1). Mutation serves its purpose of introducing extra diversity into the generations.[8] In this instance, a crossover probability of 70% and a mutation rate of 5% were chosen. A 70% crossover probability is typical for a genetic algorithm but a mutation rate of 5% is abnormally high. The mutation rate was chosen to be high because the intermediate population sizes (the population size of all generations except the first generation) were chosen to be very small. Larger intermediate populations were impractical due to the computationally intensive simulation process.

3.3.4 Convergence

The final component of a genetic algorithm is convergence. Once the offspring population has been generated, it must be analyzed for convergence. Upon convergence, an optimized individual, and thus a solution to the problem, may be ascertained. Convergence can be determined in a variety of ways as long as the optimized individual is coupled with the method of convergence that defined it. Due to the small size of offspring populations, the Student's t-distribution is used as the convergence method. Equations 10–12 are the mean, variance, and standard deviation, respectively, where x_i is the control parameter being analyzed.

$$\mu = \frac{\sum_{i=1}^{N} x_i}{N} \tag{10}$$

$$< s^2 > \; = \frac{1}{N-1} \sum_{i=1}^{N} (x_i - \mu)^2 \tag{11}$$

$$\sqrt{< s^2 >} = s \tag{12}$$

In this case, the normalized difference between any 2 control parameters (normalized parameter niche size) is 1. The convergence condition chosen for this genetic algorithm is that the standard deviation of a given control parameter must be less than twice as much of the normalized parameter niche size for a given confidence interval. Once this condition is met for all 3 control parameter sets, the optimized individual is taken as the mode of each control parameter set. Confidence in the optimized individual is established by multiplying the standard deviation of a given control parameter, in the convergence condition, by a t-distribution confidence coefficient. The greater the confidence coefficient, the greater the confidence interval. Confidence ranges on a nonlinear scale from 50% to 99.9%. For this case, the confidence interval was chosen as 90%.

4. Results and Discussion

4.1 Generations

The first generation is significant in both purpose and design. From Table 1 we see that the initial population size (31) is much larger than the intermediate population size (6). The initial population corresponds to the first generation, while the intermediate population size corresponds to every subsequent generation. Generation 1 is allowed to be significantly larger than the intermediate populations because it is random and could be applied to all 51 cases of α and M_∞. A table of control parameter values for generation 1 is displayed in Table 2.

Table 2 Control parameter values for generation 1

Individual	Q_1 (mm)	Φ_1 (°)	Φ_2 (°)
Individual 1	64.25	1.5	5
Individual 2	1.25	0	4
Individual 3	50.75	5.5	7.5
Individual 4	19.25	4	5
Individual 5	28.25	3.5	6
Individual 6	37.25	7	3.5
Individual 7	68.75	4.5	3
Individual 8	28.25	4.5	6.5
Individual 9	68.75	6.5	0.5
Individual 10	19.25	6	1
Individual 11	50.75	4.5	1
Individual 12	46.25	1	3
Individual 13	37.25	1.5	6.5
Individual 14	50.75	7	6
Individual 15	46.25	0	0
Individual 16	10.25	3.5	3
Individual 17	10.25	1	4
Individual 18	68.75	7.5	3
Individual 19	10.25	5.5	5
Individual 20	1.25	4	5
Individual 21	37.25	3.5	2
Individual 22	64.25	0	3
Individual 23	46.25	5	0
Individual 24	14.75	0	7.5
Individual 25	23.75	0.5	1
Individual 26	32.75	4	0.5
Individual 27	68.75	0.5	2.5
Individual 28	10.25	6.5	1.5
Individual 29	59.75	6.5	3.5
Individual 30	46.25	5.5	2.5
Individual 31	28.25	1	7.5

Because generation 1 was completely random and the same individuals could be used for all 51 cases, it was decided to maximize the population size (for this optimization process, populations can range from 4 to 31). Thus, the greatest benefit is obtained for the lowest cost (31 individuals processed as opposed to 1581). Therefore, only one population of 31 individuals represents generation 1 across all 51 cases. Generation 2 and beyond, however, require populations for each specific α and M_∞. As mentioned previously, this is why the intermediate population size is so small. The phenotypes of generation 2 for Mach 2 at $\alpha = 8°$ are shown in Fig. 12.

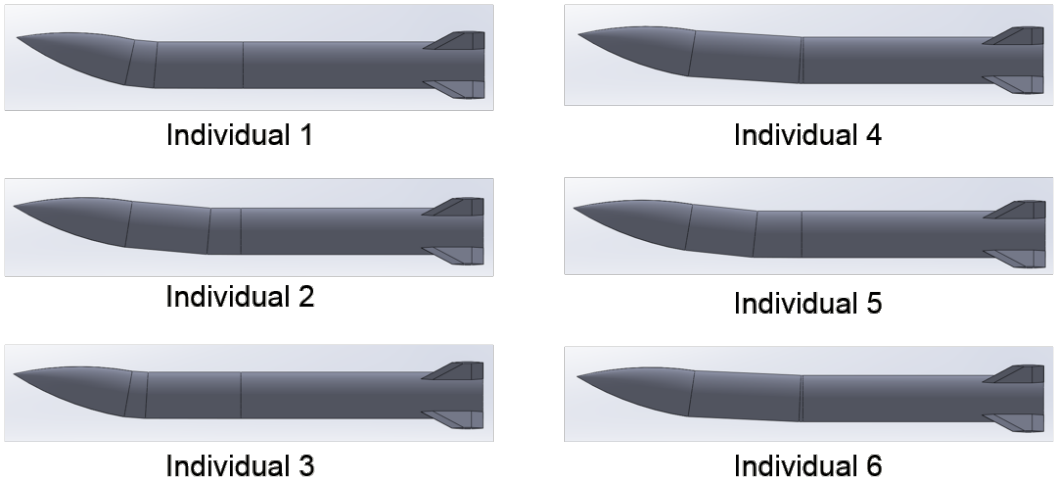

Fig. 12 Generation 2 phenotype manifestation for Mach 2 at α = 8°

4.2 Unique Cases

Among the 51 cases in the test matrix of Mach number (2, 3, and 4) and α investigated ($-8° \leq \alpha \leq 8°$), there are specific cases that offer unique results. The unique results can be determined by examining the fringes of the test matrix or by gaining a general understanding of the cases available. The unique problems at the fringes of the test matrix can be found by simply observing the test matrix, while a general understanding of the cases available can be found by analyzing the aerodynamic coefficients of a random distribution of individuals. The pitching moment coefficient as a function of α for generation 1 individuals at Mach 2 is plotted in Fig. 13.

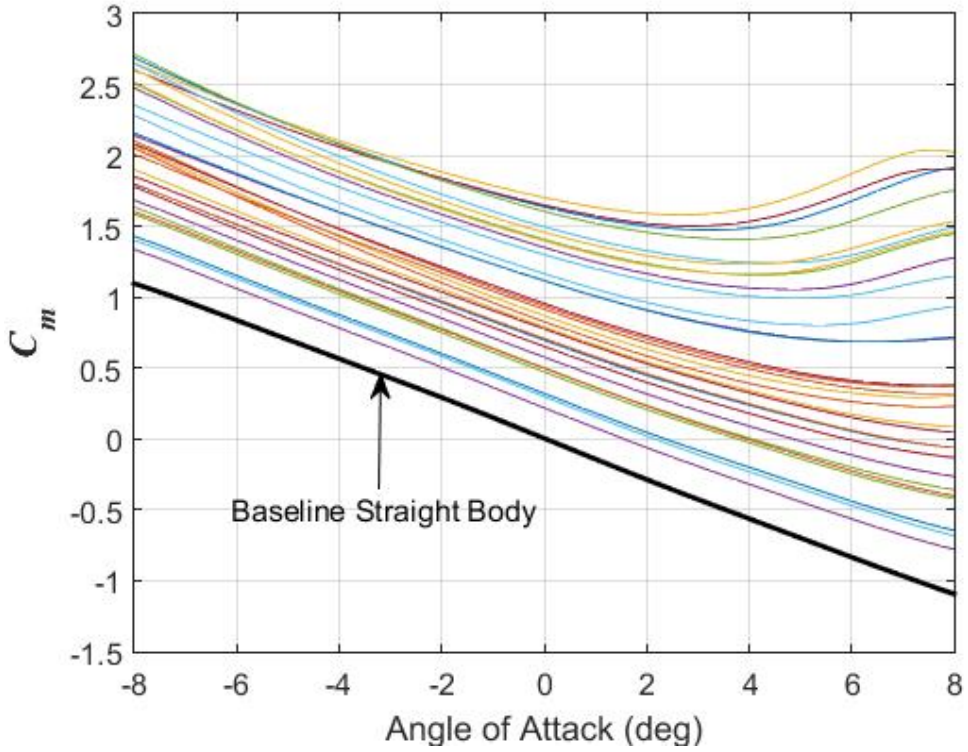

Fig. 13 Pitching moment coefficient as a function of α for generation 1 individuals at Mach 2

The fringes of the test matrix offer unique results because they are likely to demonstrate the greatest contrast between optimized individuals. For example, the geometry of optimized individual at Mach 2, $\alpha = -8°$ can be compared with that of the optimized individual found at Mach 4, $\alpha = -8°$ or at Mach 2, $\alpha = 8°$ (same α, different M_∞ or same M_∞, different α). Similarly, the optimized individual found at Mach 4, $\alpha = 8°$ could be compared with the same optimized individuals. Ideally, this will determine what makes the geometry of the optimized individual best.

Other unique cases are found by analyzing Fig. 13. Each curve on the plot represents an individual simulated across the range of angles of attack at Mach 2. The first observation that should be made is that every configuration offers a maneuverability improvement over the baseline straight body configuration. It should also be understood that this comes with a drag penalty and an increase in normal force coefficient as shown in Figs. 14 and 15. Although only data at Mach 2 are shown, Mach 3 and Mach 4 data sets show similar trends.

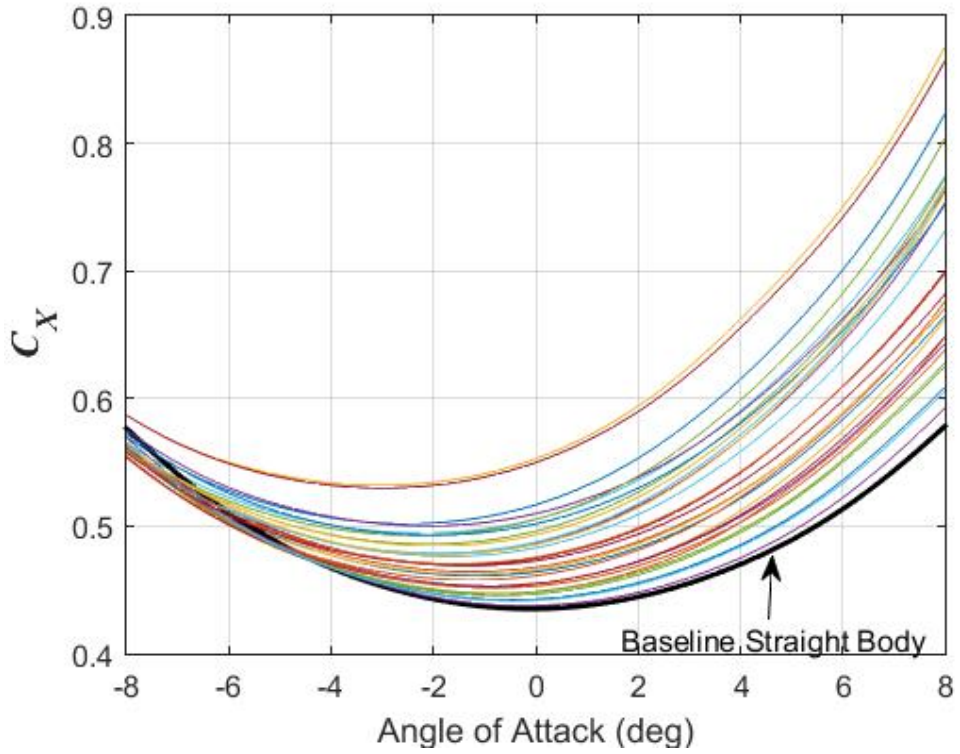

Fig. 14 Axial force coefficient as a function of α for generation 1 individuals at Mach 2

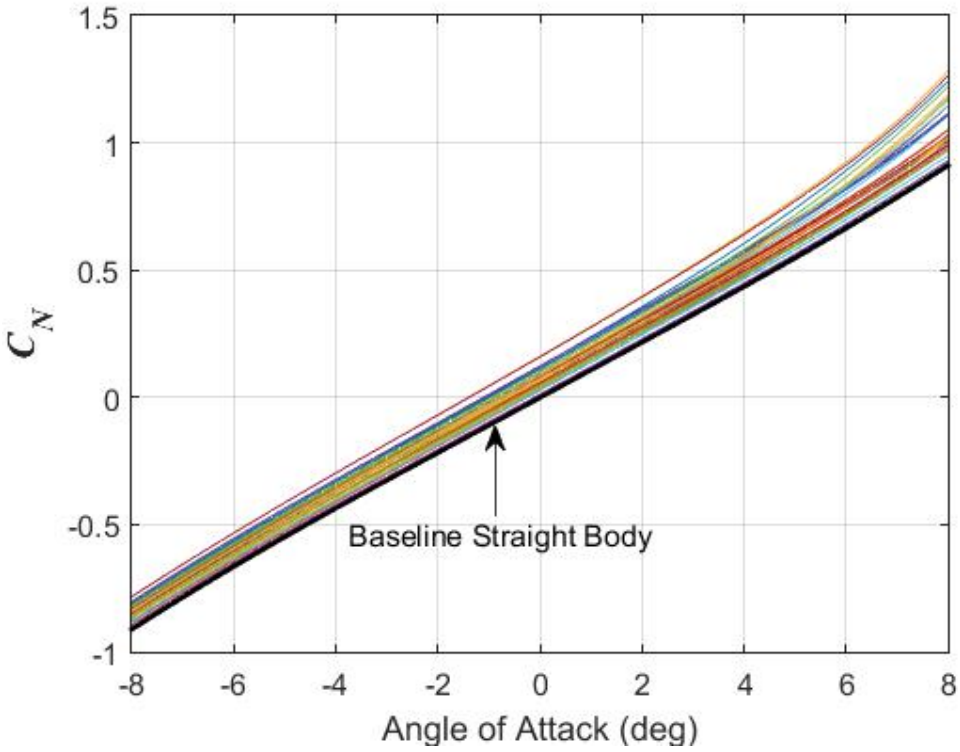

Fig. 15 Normal force coefficient as a function of α for generation 1 individuals at Mach 2

An analysis of the axial force coefficient (Fig. 14) shows that the individuals diverge drastically in the same manner that pitching moment coefficient becomes increasingly nonlinear at higher α, although the range is much smaller. This demonstrates that for increased control authority there is also increased drag, which is not unexpected. Figure 15 shows that there is little difference between individuals in normal force coefficient. The data near high angles of attack diverge slightly more than that of the axial force coefficient (set size of C_N is 46.2, while the set size for C_X is 32.1 at $\alpha = 8°$), but not to the extent that the pitching moment coefficient diverges (set size is 311.7 at $\alpha = 8°$). The large variation in C_m means that its set size and, therefore, value score are larger and have the greatest effect on the objective function. This is in addition its having the largest priority score.

Two trends in Fig. 13 highlight potentially unique cases. The most apparent case is the macroscopic trend across individuals and angles of attack. In a general sense, differences in pitching moment coefficient are linear at negative angles of attack and nonlinear at positive angles of attack. Intuitively, this makes sense because the configurations are only permitted to deflect in one direction. Thus, for a given shape, there is less projected area at negative angles of attack then at positive angles of attack. Since projected area is indirectly related to pitching moment coefficient, there will be greater diversity in pitching moment coefficient at positive angles of attack and less diversity at negative angles of attack.

The second trend, which is less significant but still important, is that the C_m curves of the individuals cross (i.e., they are not parallel). This suggests that an optimized individual for one case will not necessarily be the same as an optimized individual at a different case. This is especially true considering optimized individuals at the fringes of the test matrix.

Finally, Fig. 13 shows the optimized individual will likely result in an unstable configuration. This conclusion is drawn, as numerous individuals trim at an impractical angle or have no trim angle. These individuals would exhibit disastrously unstable longitudinal maneuverability if subjected to prolonged flight in that configuration. Therefore, the proposed flight scenario is to cruise in the baseline straight body configuration and to maneuver in the bent body configuration.

4.3 Algorithm Functionality

To ensure the algorithm is actually converging to optimized individuals, there are 2 signs to look for: decreasing standard deviation and increasing average fitness. The algorithm may not converge in the first 3 generations but convergence can still be observed. As the algorithm iterates through successive generations, individuals

within the populations will become increasingly similar. This is because the algorithm is ultimately converging to the best answer (the optimized individual). The possibility does exist that the algorithm is converging on a local optimal individual. The chance of this happening has been minimized by starting with a large initial data set, implementing a strategy that can search the entire design space, and choosing a high mutation rate. If the concern remains that a local optimal individual is being reached, an evaluation of the parameters searched could be conducted to ensure that there are no significant gaps in the search. This final parameter evaluation has not been implemented at this time.

In this particular case, generations 1 and 2 at Mach 2 can be analyzed. Generation 1 is represented by 1 population of 31 individuals; generation 2 is represented by 51 populations (17 angles of attack and 3 Mach numbers) of 6 individuals. Each individual represents 3 control parameters (Q_1, Φ_1, Φ_2). Therefore, generation 1 is defined by 93 control parameter values and generation 2 is represented by 918 control parameter values. The results are analyzed assuming that all 51 populations of generation 2 should decrease uniformly in standard deviation.

Using the same notation from Fig. 2, the control parameters' statistics are displayed in Fig. 16. As mentioned earlier, on a normalized set scale, each control parameter becomes an integer between 1 and 16. This allows statistical comparison across any control parameter from any population within any generation. Generation 1, as expected, is evidently random because the mean values are close to the median value of the design space. As a second characteristic of a random population, the standard deviation is almost uniform across the control parameters.

Generation 1

Mean Std. Dev.	4.71

	Q_1	Φ_1	Φ_2
Mean	8.97	8.19	8.10
Std. Dev.	4.71	4.89	4.52

Generation 2

Mean Std. Dev.	3.69

22% reduced standard deviation

Angle of Attack	AOA -8°	AOA -7°	AOA -6°	AOA -5°	AOA -4°	AOA -3°	AOA -2°	AOA -1°	AOA 0°	AOA 1°	AOA 2°	AOA 3°	AOA 4°	AOA 5°	AOA 6°	AOA 7°	AOA 8°
Mean Standard Deviation	3.77	3.95	3.85	4.21	2.82	2.99	2.88	2.55	4.63	4.57	4.34	4.54	3.43	2.21	4.13	4.27	3.60

Fig. 16 Statistical comparison between generations 1 and 2 at Mach 2

At the bottom of Fig. 16, we see the mean standard deviation within each population for each α. From these averages, it is obvious there is no correlation between the populations. Despite only analyzing 1 iteration of the algorithm with almost 1000 control parameters, it is concluded that the algorithm is converging because the mean standard deviation across all the control parameter values has decreased by an average of 22%.

To ensure that successive generations are achieving increased performance, the fitness scores must be compared carefully. The fitness scores (calculated by the objective function) within each generation are only relevant to their respective generation because the objective function also considers the size of each set of aerodynamic coefficients (niche is taken as 0.01). This metric is dynamic throughout the algorithm so comparing the calculated fitness scores is meaningless. Comparisons of fitness scores become valid when average value of a coefficient is taken from one generation and its value score calculated within the coefficient set (min, max, set size) of another generation. The fitness comparison is made in this manner between generations 1 and 2 at Mach 2, $\alpha = 8°$ in Tables 3 and 4. Figure 17 shows the set size of each of the aerodynamic coefficients has significantly decreased between generations 1 and 2 at Mach 2, $\alpha = 8°$. Even after just 2 generations, the benefit of the genetic algorithm is apparent.

Table 3 Aerodynamic coefficient value comparison between generations for Mach 2, α = 8°

Aerodynamic coefficients	Generation 1 (Average)	Min	Max	Set size	Generation 2 (Average)	Set size
C_m	0.49	–1.09	2.02	311.73	1.16	85.69
C_N	1.14	0.93	1.39	46.24	1.24	15.75
C_X	0.59	0.45	0.77	32.11	0.60	10.02

Table 4 Fitness score calculation comparison between generations for Mach 2, α = 8°

Generations	C_X Value score	C_N Value score	C_m Value score	Final fitness score
1	24.34	37.77	75.41	52.11
2	23.82	41.14	179.26	104.43

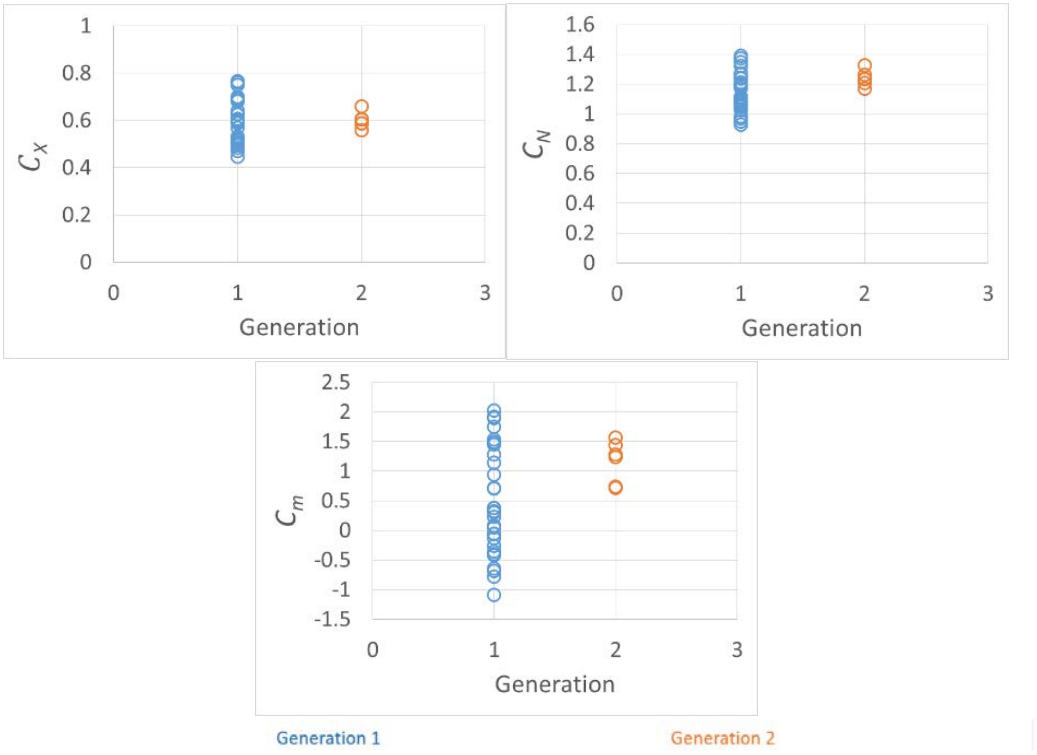

Fig. 17 Aerodynamic coefficient evolution across generations 1 and 2 for Mach 2, α = 8°

Not surprisingly, generation 2 shows increased performance. What is surprising is by how much and why. The final fitness score has increased by over 100% from generation 1 to generation 2 when generation 2 is considered within the coefficient set of generation 1. This remarkable improvement can be attributed to both the effective optimization of the algorithm and the nature of the problem. From Fig. 13, it is concluded that the greatest spread in pitching moment coefficient occurs at the highest angles of attack. Therefore, more improvements can be expected at higher angles of attack compared with lower angles of attack.

Table 3 shows that the pitching moment coefficient was improved the most by the vector-evaluated genetic algorithm between generations 1 and 2. It also had the greatest impact on directing the shape of the projectile in this iteration due to it having the largest set size (range of values). The highest priority coefficient was given to $C_{m,}$ as it was believed that the pitching moment coefficient was important, but the inherent importance further emphasized the metrics' influence on projectile shape. Simultaneously, the other coefficients had a much lower influence on the shape of the projectile. This is not only evident by the substantially smaller set sizes but also the changes in average coefficient value across generations (although this is also influenced by the lower priority coefficient). The axial force coefficient actually increased despite desired minimization, while the normal force coefficient only increased slightly. The increase in C_x is undesirable but also necessary, as this

is a small sacrifice allowed for larger C_m values. Unfortunately, this is only one particular case out of the 51 different cases and it cannot be assumed that it is representative of the entire test matrix. It is possible that by using multi-objective optimization rather than vector-evaluated optimization that C_x could truly be minimized while maximizing C_m. However, the currently vector-evaluated optimization should provide a sufficiently good answer from which to determine if enough maneuver authority could be generated.

5. Conclusion

Unique cases of bending body projectiles as well as genetic algorithm functionality for vector-evaluated optimization were analyzed for generations 1 and 2 at Mach 2. The resulting analysis revealed that fringes of the test matrix suggest further research will show unique differences in the optimized individuals. A deeper investigation discovered that nonlinear sections of the aerodynamic coefficient data also suggest unique cases within the test matrix. Algorithm functionality shows great promise with an observed decrease in standard deviation and an observed increase in fitness score. This is strong evidence, although not concrete, that the algorithm is not only converging, but also converging to a globally optimized individual.

Further research that needs to be completed includes optimization of the entire test matrix and analysis of the flow field of optimized individuals to compare with the baseline straight body configuration. This comparison should expose why optimized individuals exhibit increased performance compared with the straight body configuration. The projectile concept might also be improved by transitioning away from discrete, rigid bends and toward a continuous curve. Bezier control points offer a method of modeling a continuous shape while still using the discrete control points required for the genetic algorithm. A continuous projectile shape may have improved drag performance, but may prove more difficult to control because the location of the expansion fan could wander along the curve. More analysis needs to be done to conclude the optimal curve or number of bends required to maximize maneuverability and controllability.

6. References

1. Youn EB, Silton SI. Numerical study on bending body projectile aerodynamics. 34th Applied Aerodynamics Conference; 2016 June 13–17; Washington, DC. AIAA 2016-4331.

2. Silton SI, Fresconi FE. The effect of canard interactions on aerodynamic performance of a fin-stabilized projectile. 53rd AIAA Aerospace Sciences Meeting; Kissimmee, FL; 2015 Jan 5–9; AIAA 2015-1924.

3. Blair AB. Wind tunnel investigation at supersonic speeds of a canard controlled missile with fixed and free-rolling tail fins. Hampton (VA): National Aeronautics and Space Administration; 1978 Sep. NASA Technical Paper 1316.

4. Ericsson LE, Reding JP. Steady and unsteady vortex-induced asymmetric loads on slender bodies. J of Spacecraft and Rockets. 1981;18(2):97–109.

5. Landers MG, Hall LH, Auman LM, Vaughn ME Jr. Deflectable nose and canard controls for a fin-stabilized projectile at supersonic and hypersonic speeds. 21st AIAA Applied Aerodynamics Conference; 2003 June 23–26; Orlando, FL. AIAA 2003-3805.

6. Reinecke WG. Aerodynamic coefficients for extending and bending projectiles. 23rd International Symposium on Ballistics. 2007 Apr 16–20; Tarragona, Spain.

7. Shoesmith B, Birch T, Mifsud M, Meunier M, Shaw S. CFD analysis of a supersonic projectile with deflectable nose control. 3rd AIAA Flow Control Conference; 2006 June 5–8; San Francisco, CA. AIAA 2006-3200.

8. Li J, Wray TJ, Agarwal RK. Shape optimization of supersonic bodies to reduce sonic boom signature. 34th AIAA Applied Aerodynamics Conference; 2016 June 13–17; Washington, DC. AIAA 2016-3432.

9. Upender KK, Nguyen NT. Lift optimization study of a multi-element three-segment variable camber airfoil. 34th AIAA Applied Aerodynamics Conference; 2016 June 13–17; Washington, DC. AIAA 2016-3569.

10. Xiaoming F, Yufei Z, Chen H. Transonic nacelle aerodynamic optimization based on hybrid genetic algorithm. 34th AIAA Applied Aerodynamics Conference; 2016 June 13–17; Washington, DC. AIAA 2016-3833.

11. Koreanschi A, Gabor OS, Acotto J, Botez RM, Mamou M, Mebarki Y. A genetic algorithm optimization method for a morphing wing tip demonstrator validated using infra red experimental data. 34th AIAA Applied Aerodynamics Conference; 2016 June 13–17; Washington, DC. AIAA 2016-4037.

12. Fonseca CM, Fleming PJ. Genetic algorithms for multiobjective optimization: formulation, discussion and generalization. Genetic Algorithms: Proceedings of the Fifth International Conference; 1993 July; San Mateo, CA.

13. Dupuis AD, Hathaway W. Aeroballistic range tests of the Air Force Finner reference projectile. Valcartier (Quebec, Canada): Defense R&D Canada; 2002 May. Report No.: TM 2002-008.

14. West KO. Comparison of free flight spark range and wind tunnel test data for a generic missile configuration at Mach numbers from 0.6 to 2.5. Eglin Air Force Base (FL): Air Force Armament Laboratory (US); 1981 Oct. Report No.: AFATL-TR-81-87.

15. West KO, Whyte RH. Free flight and wind tunnel test of a missile configuration at subsonic and transonic Mach numbers with angles of attack up to 30 degrees. 11th Navy Aeroballistic Symposium; 1978 Aug; Warminster, PA.

16. Jenke LM. Experimental roll-damping, magnus, and static-stability characteristics of two slender missile configurations at high angles of attack (0–90 deg) and Mach numbers 0.2 through 2.5. Arnold Air Force Base (TN): Arnold Engineering and Development Center (US); 1976 July. Report No: AEDC-TR-76-58.

17. Bhagwandin V. High-alpha prediction of roll damping and magnus stability coefficients for finned projectiles. J of Spacecraft and Rockets. 2016 Jul–Aug;54:720–729.

18. Bhagwandin V, Sahu J. Numerical prediction of pitch damping stability derivative for finned projectiles. J of Spacecraft and Rockets. 2014 Sep–Oct;51:1603–1618.

19. Rosema C, Doyle J, Blake W. Missile Datcom user's manual – 2014 revision. Flight Dynamics Directorate, Wright Patterson Air Force Base (OH): Air Force Research Laboratory (US); 2015 Dec. Report No: AFRL-RQ-WP-TR-2014-0281.

20. Sobachkin A, Dumnov G. Numerical basis of CAD-embedded CFD. Waltham (MA): Dassault Systemes – SOLIDWORKS; 2014 Feb.

21. Metacomp. CFD^{++}. Agoura Hills (CA): Metacomp Technologies Inc. [accessed 2016 Aug 2]. http://www.metacomptech.com/index.php/products/cfd.

22. Metacomp. Multipurpose intelligent meshing environment. Agoura Hills (CA): Metacomp Technologies Inc. [accessed 2016 Aug 2]. http://www.metacomptech.com/index.php/products/mime.

23. Sahu J, Heavey K. Time-accurate computations for rapid generation of missile aerodynamics. Atmospheric Flight Mechanics Conference; 2010 Aug 2–5; Toronto, Ontario, Canada. AIAA-2010-8248.

24. Schaffer JD. Multiple objective optimization with vector evaluated genetic algorithms. In: Grefenstette JJ, editor. Proc First Int Conf on Genetic Algorithms; 1985; Hillsdale (NJ): Lawrence Erlbaum Associates Inc. p. 93–100.

25. Xia X. Particle swarm optimization method based on chaotic local search and roulette wheel mechanism. 2012 International Conference on Applied Physics and Industrial Engineering; 2012; Beijing, China. ICAPIE 1875-3892.

26. Lipowski A, Lipowska D. Roulette-wheel selection via stochastic acceptance. Physica A. 2012:391.

27. Ghate A, Smith RL. Adaptive search with stochastic acceptance probabilities for global optimization. Operations Research Letters. 2008;36(3):285–290.

List of Symbols, Abbreviations, and Acronyms

M_∞	freestream Mach number
C_m	pitching moment coefficient
C_N	normal force coefficient
C_X	axial force coefficient
F_N	normal force
F_X	axial force
p_∞	freestream pressure
$< s^2 >$	variance
3-D	3-dimensional
AFF	Air Force Finner
CAD	computer-aided design
CFD	computational fluid dynamics
CG	center of gravity
D	projectile diameter
DOD	Department of Defense
FSB	Flight Sciences Branch
HPCMP	High Performance Computing Modernization Program
M	pitching moment
MIME	Multipurpose Intelligent Meshing Environment
N	number of individuals in a given generation
Q_1	location of the second bend relative to CG
S	area of the projectile
s	standard deviation
w_i	final fitness score of an individual
w_{max}	maximum final fitness score of the generation

μ	mean value
Φ_1	first bend angle
Φ_2	second bend angle
α	angle of attack
γ	gas constant for air

1 (PDF) DEFENSE TECHNICAL INFORMATION CTR DTIC OCA

2 (PDF) DIRECTOR US ARMY RESEARCH LAB RDRL CIO L IMAL HRA MAIL & RECORDS MGMT

1 (PDF) GOVT PRINTG OFC A MALHOTRA

5 (PDF) AMRDEC L AUMAN J DOYLE K KENNEDY M MCDANIEL C ROSEMA

6 (PDF) ARDEC M STOLK Y CHEN T RECCHIA D HOSIER M DUCA G RODEBAUGH

31 (PDF) DIR USARL
RDRL WM
B FORCH
S KARNA
S SCHOENFELD
J ZABINSKI
RDRL WML
W OBERLE
P PEREGINO
A RAWLETT
RDRL WML B
J MORRIS
N TRIVEDI
RDRL WML C
S AUBERT
RDRL WML D
R BEYER
Z WINGARD
RDRL WML E
V BHAGWANDIN
I CELMINS
J DESPIRITO
F FRESCONI
J L PAUL
J SAHU
S SILTON
P WEINACHT
J VASILE
RDRL WML F
T BROWN
M ILG
B KLINE
J MALEY
B NELSON
RDRL WML G
M MINNICINO
J SOUTH
RDRL WML H
J NEWILL
RDRL WMM
M VANLANDINGHAM
RDRL WMP
D LYON